APCC
APEC CLIMATE CENTER

RESEARCH REPORT

APCC
APEC CLIMATE CENTER

PREFACE

It is our pleasure to present this report on the APEC Climate Center (APCC)'s research activities in 2013, which has been a very productive year for our Center.

APCC has expanded its research scope, in response to regional societal and scientific needs. While building expertise in climate prediction remains a priority, we are extending our reach to include policy-relevant climate applications and value-added climate information products.

APCC has accelerated efforts to better our service to the region. As one of the main services provided by APCC, the MME 3-month prediction information has been productively applied by scientists in developing countries that are unable to produce their own prediction information. Furthermore, in order to better prepare for climate-related hazards in a timely manner, APCC launched its 6-month MME prediction service in September 2013. We also began to release forecasts of the Boreal Summer Intraseasonal Oscillation (BSISO), starting from July 2013, as the world's first operational BSISO forecast service. Our researchers also achieved great success in publishing their papers in noted academic journals. Dr. Ok-Yeon Kim, for example, published a paper in *Climate Dynamics* and her research was later selected as one of the Research Highlights by another distinguished journal, *Nature Climate Change*. The following research report provides more information about our research outcomes from 2013.

We will continue to promote the best use of our research outcomes in various scientific and application areas. Our successes and achievements would not have been possible without the support of our valued partners. In this regard, I extend my thanks to you and I hope you enjoy this 2013 Research Report.

Chin-Seung Chung
Director, APEC Climate Center

CONTENTS

APCC

RESEARCH REPORT 2013-02

Revision of Climate Change by Dynamic Downscaling over the Maritime Continents

Dr. Hongwei Yang | Climate Analysis Team

ABSTRACT

Multi-decadal high-resolution dynamic downscaling over the CORDEX Southeast Asia domain were performed using the regional model WRF forced by the ERA-40 reanalysis dataset as well as the present climate and future projections (RCP4.5, RCP8.5) of the Met Office Hadley Centre's HadGEM2-AO. The downscaled low-level circulation and precipitation in the hindcast experiment, historical run, near future changes, and far future changes were analyzed and compared to observations or corresponding large-scale forcing.

In the hindcast experiment, the added values of dynamic downscaling over land exceeded those over ocean owing to the precisely described underlying surface over land considered in the WRF model. The added values over land increased when the small islands were neglected. The poor performance of the WRF model over small islands degraded the general skill over the entire land region. Although the hindcast experiment showed biases in low-level circulation fields, which can probably be attributed to the air-sea interaction being neglected, the WRF model has reliable skills for the big lands when it was driven by the "perfect" lateral boundary forcing from the reanalysis dataset.

The historical downscaling enhanced the low-level circulation biases in the driving fields from HadGEM2-AO because the regional model was unable to reduce the uncertainties in the lateral boundary forcing. Therefore, the biases in the historical downscaling were larger than those in the hindcast downscaling forced by the reanalysis dataset. However, the precipitation biases over land in the HadGEM2-AO model were reduced in the historical downscaling largely because the dominant forcing from the underlying surface over land was represented better in the fine-resolution model. The historical downscaling showed poor added value over the ocean.

Over all, the uncertainty in the RCP4.5 projection for JJA was the highest among all the cases. The mean precipitation change in the HadGEM2-AO model was more likely enhanced by the WRF model in the far future than in the near future. The uncertainty in precipitation variability projection is larger than that in the mean precipitation projection.

1. INTRODUCTION

The Maritime Continent is the region of Southeast Asia (SEA) between the Indian and Pacific Oceans and comprising thousands of islands, including Sumatra, Borneo, Java, and New Guinea, and shallow seas surrounded by a warm ocean named Tropical Warm Pool. Owing to the complex land-sea contrasts, with several big islands higher than 2000 m, large amounts of energy are transferred up into the atmosphere through the most prominent diurnal cycle (Kikuchi and Wang, 2008; Sato et al. 2009); this

is accompanied by latent heat release and gravity wave disturbances. Deep cumulus convection and heavy precipitation systems not only influence global and regional scale processes such as monsoon, MJO, and ENSO (Chang et al. 2005), but also are modulated by these processes (Ichikawa and Yasunari 2008; Qian et al. 2010).

The global model future climate projection predicts the mean temperature in the Maritime Continent to increase by 2-5 °C (Susan 2007). Mean precipitation is likely to change significantly by the end of the 21st century. Thus, the Maritime Continent is highly vulnerable to the impacts of climate change. However, global models do not always resolve the important topographic features that determine the spatial variability of rainfall at regional scales. The local error in the model over the Maritime Continent leads to systematic global uncertainties in medium-range weather prediction and climate simulation through planetary wave propagation (Peatman et al. 2013). Neale and Slingo (2003) observed that a heating anomaly over the Maritime Continent generates Rossby waves through the divergent outflow in the model, and these waves significantly affect the thermodynamic flow over North America and the northeast Eurasian region in winter. Qian (2008) found a dry bias accompanied by an eastward misplaced upper-atmospheric velocity potential in a global model simulation.

The complicated thermodynamic and circulation forcing over the Maritime Continent create large difficulties in hydrological and agriculture management. High-resolution information is necessary for developing warning systems. High-resolution regional climate downscaling (RCD) of climate change projection is essential to analyze the potential climatic impacts and adaptation measurements. A high-resolution model can capture the local features that arise from uplift condensation due to the topography (Qian and Zubair 2010); this improves the predictive performance of the amplitude of the diurnal cycle and mean rainfall (Wu and Hsu 2009; Love et al 2011; Dirmeyer et al. 2012) and even the ratio of stratiform to convective precipitation (Boyle and Klein 2010). Fine-grid experiments not only reflect the important topographic effects, but also project consistent signs of climate change (Smith et al. 2013).

Therefore, the COordinated Regional climate Downscaling EXperiment (CORDEX) was established; it aims at improving the coordination of international efforts in RCD

research. Despite the increase in organized RCD activities in most regions where CORDEX has been implemented, the RCD activity in SEA is minimal and uncoordinated. Hence, the CORDEX Southeast Asia (CORDEX-SEA) project has been established. The regional downscaling of climate projection over the Maritime Continent will provide improved high-resolution climate project information for the hydrological studies and for the agriculture sector. The hindcast and historical downscaling experiments for current climate will be forced by reanalysis data and global model output, respectively. Two climate change downscaling processes will be driven by the global model projections. The data, the evaluation method, and the experiments are described in Sections 2 and 3. The results are described in Section 4. Section 5 presents the conclusions.

2. MODEL AND DATA

The Weather Research and Forecast (WRF3.5) model (Skamarock et al. 2005), a primitive equation limited-area model under sigma coordinates, is used in this study. WRF is a regional prediction and downscaling system designed to meet both operational forecasting and atmospheric research needs. It has an advanced software architecture allowing parallel computing and system extensibility. The development of the state-of-the-art WRF has been undertaken as a collaborative project by mainly the National Center for Atmospheric Research, the Forecast Systems Laboratory, the National Oceanic and Atmospheric Administration, National Centers for Environmental Prediction, the Air Force Weather Agency, the Naval Research Laboratory, the University of Oklahoma, and the Federal Aviation Administration. WRF allows researchers to conduct simulations reflecting either real data or idealized configurations. WRF is suitable for many applications of different scales ranging from meters to thousands of kilometers. Such applications include research and operational numerical weather prediction (NWP), data assimilation and parameterized-physics research, downscaling climate simulations, driving air quality models, atmosphere-ocean coupling, and idealized simulations of phenomenon such as boundary-layer eddies, convection, and baroclinic

waves. There are two dynamics solvers in the WRF Software Framework (WSF): the Advanced Research WRF (ARW) solver (originally referred to as the Eulerian mass or "em" solver) developed primarily at NCAR, and the Nonhydrostatic Mesoscale Model (NMM) solver developed at NCEP. We chose the ARW solver in this study. The governing equations of the ARW dynamics solver are the compressible, nonhydrostatic Euler equations. The equations are written in flux form, and its variables satisfy conservation equations, following the philosophy of Ooyama (1990). Further, the equations are expressed by using a terrain-following mass vertical coordinate (Laprise, 1992). In this model, the top surface is a constant pressure surface; we consider this surface to be at 50 hPa pressure. Arakawa C-grid staggering is applied for the horizontal grid. A 3rd order Runge-Kutta scheme with a smaller time step for acoustic and gravity-wave modes is applied for time-split integration (Klemp and Wilhelmson 1978; Skamarock and Klemp 1992; Wicker and Skamarock 2002). WRF offers multiple physical options that can be combined in any way (Skamarock et al. 2005).

In our study, we choose WRF Single-Moment 6-Class Microphysics (WSM 6)-class graupel scheme (Hong et al. 2004) as the microphysics parameterization; this scheme includes six types of hydrometeors, namely, water vapor, cloud water, rain, cloud ice, snow, and graupel in six different arrays. Thus, it allows the existence of supercooled water, and a gradual melting of the snow below the melting layer. We introduce a new method for representing mixed-phase particle fall speeds weighted by the mixing ratios for the snow and graupel particles by assigning a single fall speed to both; this fall speed is applied to both sedimentation and accretion processes. We choose the modified Tiedtke scheme (Tiedtke 1989; Zhang et al. 2011) as the cumulus parameterization; this scheme is a mass-flux type scheme with CAPE-removal time scale, shallow component, and momentum transport. Land surface parameterization follows the Unified Noah land-surface model (Tewari et al. 2004), which is a unified NCEP/NCAR/AFWA scheme with soil temperature and moisture in four layers, fractional snow cover, and frozen soil physics. The Yonsei University (YSU: Hong et al. 2006) planetary boundary layer (PBL) is employed here; here, the counter gradient terms are used to represent fluxes owing to non-local gradients. The surface layer scheme is the MM5 Monin-Obukhov scheme (Paulson 1970; Dyer and Hicks 1970; Webb 1970; Beljaars 1994; Zhang and Anthes 1982), which is based on the Monin-Obukhov scheme

with a Carslon-Boland viscous sub-layer and standard similarity functions from look-up tables. Long wave and short wave radiative transfer model follows the CAM scheme (Collins et al. 2004), which is based on the CAM 3 climate model used in CCSM; it takes into account the contributions of aerosols and trace gases and uses yearly CO_2, and constant N_2O (311E-9), and CH_4 (1714E-9).

The lateral boundary forcing fields included geopotential height, air temperature, specific humidity, and horizontal winds. The width of the buffer zone in our model was set to be 10 grid points, where the prognostic variables of WRF model were nudged toward the large-scale forcing fields following the method of Davies and Turner (1977) with Newtonian nudging and horizontal diffusion within the RCM buffer zones. The initial state conditions are as follows: surface pressure, sea-level pressure, 2-m height moisture, 2-m height temperature, 10-m height horizontal winds, soil moisture, soil temperature, and skin temperature. The skin temperature over the ocean was considered sea surface temperature. We obtained 30' horizontal resolution topography and land use data in Noah LSM from the U.S. Geological Survey. The 30' soil type data were obtained from the State Soil Geographic (STATSGO) Database, and 5'' global data were obtained from the Food and Agriculture Organization of the United Nations.

ERA-40 (Uppala et al. 2005) reanalysis dataset was used for the large-scale forcing fields for the hindcast experiment. The output of HadGEM2-AO (Baek et al., 2012) global coupled model was used for the large-scale forcing fields for the historical experiment and future projection experiments. To verify the simulated circulation fields in our hindcast and historical experiments, the seasonal mean ensemble of reanalysis datasets NCEP-R2 (Kanamitsu et al. 2002), ERA-40, and JRA-25 (Onogi et al. 2007) was used as reference data. Seasonal mean ensemble precipitation from GPCP (2.5° × 2.5°; Adler et al. 2003), CMAP (2.5° × 2.5°; Xie and Arkin 1996), and the Tropical Rainfall Measuring Mission (TRMM3B43, 0.25° × 0.25°; Huffman et al. 2007) over ocean, as well as ensemble of TRMM3B43, the gauge-based analysis CRU (0.5° × 0.5°; New et al., 2002), and APHRODITE (0.5° × 0.5°; Yatagai et al. 2009) over land were used as the truth data for rainfall to evaluate the precipitation in our hindcast and historical experiments. Compared with the ensemble of observed precipitation,

the added values in the downscaling of hindcast and historical experiments were investigated through the temporal correlation coefficient, temporal root mean square error, spatial running correlation coefficient, and spatial root mean square error in March-May (MAM), June-August (JJA), September-November (SON), and December-February (DJF) seasons. The near and far future changes of mean and spatial variability in precipitation in RCP4.5 and RCP8.5 were analyzed.

3. EXPERIMENTAL DESIGN

The tropical climate over the Maritime Continent is very important and unique as it is located in the most active convective area of the world and is influenced by both the Hadley and Walker circulations. The Maritime Continent consists of more than 10,000 islands with high topography.

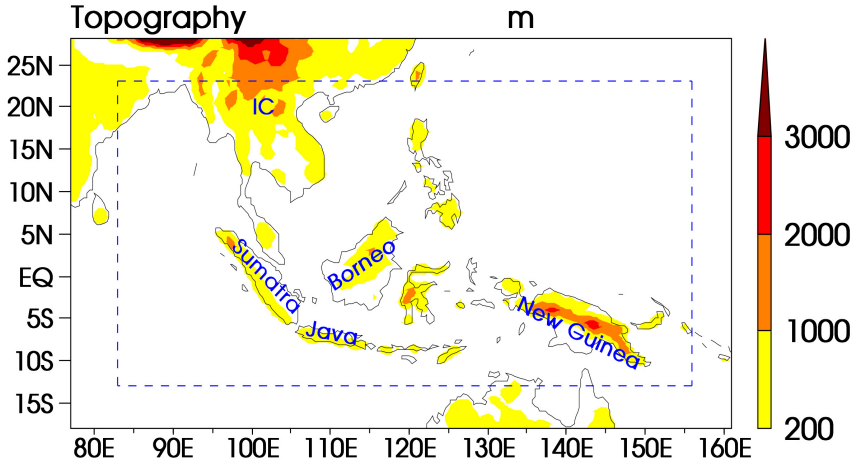

Figure 1 Simulation domain (18°S-29°N, 76-160°E), buffer zone (outside of blue dashed lines:13°S-23°N, 83-156°E), and topography (color shading in units of meters). Analysis areas over land enclosed by blue lines refer to IC, Sumatra, Java, Borneo, and New Guinea.

To consider the climate system, we require a sufficiently large domain size, where the regional model could develop its own dynamics, and sufficient computational resource; we designed our model domain covering the Maritime Continent region to extend from 18°S to 29°N and from 76°N to 160°E (Fig. 1). We choose the cylindrical equidistant map projection with a zonal and meridional grid space of approximately 0.44°. The model has 185 west-east and 113 south-north grid points, and 31 sigma layers in the vertical direction up to 50 hPa.

Four experiments named hindcast experiment, historical experiment, Down-45, and Down-85 were designed and they were initiated and forced by the ERA-40, HadGEM2-AO historical run, HadGEM2-AO RCP4.5, and HadGEM2-AO RCP8.5 future projections, respectively. The prescribed SST was from the same dataset of the lateral boundary forcing for each experiments. Here the prefix "Down" in the experimental names refers to downscaling. The historical experiment is our control experiment, and its output is used as the reference data for the climate change. The ERA-40 is available at 6-h intervals with a horizontal resolution of 2.5° and 17 pressure levels. The output of HadGEM2-AO is a 6-hourly data with a horizontal resolution of 1.25° in latitude and 1.875° in longitude. The physical parameterization scheme and model configuration were kept the same for all experiments. All model parameters were considered with their default values without tuning.

The hindcast experiment was run from 1 January 1980 to 31 December 2001. The historical experiment was run from 1 January 1970 to 31 December 2005. Down-45 and Down-85 were run from 1 January 2006 to 31 December 2100. The first year of the hindcast and historical experiments were considered as a "spin-up" period, and the model outputs from the second year were analyzed. The near and far futures were defined as periods from 2021 to 2050 and from 2071 to 2100, respectively. The historical reference data for studying climate change were taken for the period 1971-2000, a sub-period of the period of the historical experiment.

4. RESULTS

4.1 Hindcast experiment

1) Low-level circulation

To evaluate the circulation fields simulated in the hindcast experiment, we took the ensemble mean of three reanalysis datasets as the reference dataset. The three reanalysis datasets are the NCEP-R2, ERA-40, and JRA-25.

In MAM, an anticyclone bias centered at the Bay of Bengal (BOB) accompanied by a positive geopotential height anomaly located to its northeast over the Indochina peninsula at 850 hPa pressure level was observed in the hindcast experiment results (Fig. 2a). Over New Guinea and its surrounding ocean, another positive geopotential height anomaly was observed with a southwesterly anomaly to its north. The entire geopotential height showed positive anomaly in east and negative anomaly in west. In JJA (Fig. 2b), a strong cyclone anomaly centered at the South China Sea (SCS) and a weak negative geopotential height anomaly centered at the BOB were generated in the WRF model. The generation of the strong cyclone anomaly over the SCS may be attributed to the lack of air-sea interaction in the hindcast experiment, in which the sea surface temperature (SST) is prescribed in the WRF model using the SST from the reanalysis dataset. This is because the atmosphere-only model cannot adjust the SST owing to the model's errors in the monsoon-ocean interactive system (Fu et al. 2002; Fu and Wang 2004). In SON, a weak cyclone circulation anomaly was present over the SCS and the Philippine Sea; this may be attributed to the prescribed SST (Fig. 2c). In DJF, the anomalous pattern in the low-level circulation was similar to that in MAM (Fig. 2d).

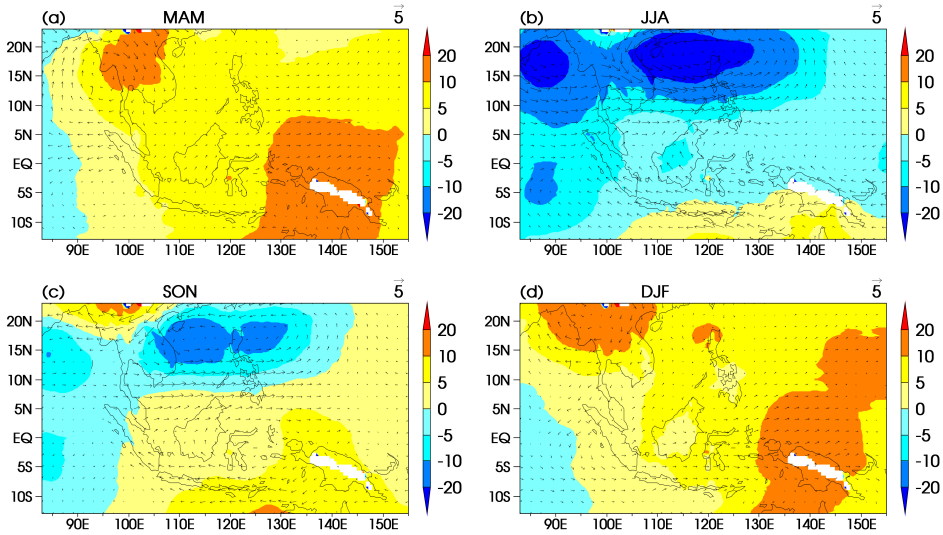

Figure 2 The model biases of geopotential height (shading in units of meter) and horizontal winds (vector in units of 5 m s-1) at 850 hPa in MAM mean (a), JJA mean (b), SON mean (c), and DJF mean (d), in the hindcast experiment forced by ECMWF 40-year reanalysis (ERA-40). All the biases are defined by the departure of RCM simulations from the large-scale forcing of ensemble mean of the NCEP/DOE reanalysis 2 (NCEP-R2), ERA-40, and the Japanese 25-year reanalysis (JRA-25). White zones are the missing value masked by the topography.

2) Precipitation

To verify the simulated precipitation in the hindcast experiment, the observed climatological seasonal mean of rainfall was used as the reference dataset; this dataset was derived from the ensemble mean of CRU, APHRODITE, TRMM over land, CMAP, GPCP, and TRMM over ocean.

The WRF model showed the added values only in JJA and SON over the entire domain in terms of the correlation coefficient of spatial distribution of the climatological seasonal mean rainfall (Tab. 1). These added values corresponded to land instead of the ocean in JJA and SON. The correlation coefficients are 0.62 (0.43) in JJA and 0.61 (0.30) in SON for the hindcast experiment (ERA-40) over the land.

Table 1 Spatial correlation coefficients (Rs) of seasonal precipitation of the ERA-40 and hindcast downscaling experiments relative to the observation in MAM, JJA, SON, and DJF, over entire domain, land regional and ocean area.

Rs(GCM/RCM)	all	land	ocean
MAM	0.71 \ 0.68	0.58 \ 0.54	0.79 \ 0.72
JJA	0.74 \ 0.75	0.43 \ 0.62	0.85 \ 0.80
SON	0.68 \ 0.75	0.30 \ 0.61	0.81 \ 0.78
DJF	0.82 \ 0.79	0.73 \ 0.68	0.86 \ 0.83

In terms of root mean square error (RMSE) of the climatological seasonal mean precipitation (Tab 2), the hindcast experiment showed added values in all seasons over the land. Over the ocean, the hindcast experiment showed added values only in MAM and DJF.

Table 2 Spatial root mean square error (Es, in unit of mm d^{-1}) of seasonal precipitation of the ERA-40 and hindcast downscaling experiments relative to the observation in MAM, JJA, SON, and DJF, over entire domain, land regional and ocean area.

Es(GCM/RCM)	all	land	ocean
MAM	3.77 \ 2.65	5.80 \ 3.31	3.16 \ 2.48
JJA	3.49 \ 6.20	5.22 \ 4.75	3.00 \ 6.46
SON	3.95 \ 4.07	5.92 \ 3.34	3.39 \ 4.21
DJF	3.71 \ 3.25	5.15 \ 4.10	3.31 \ 3.03

The added values of dynamic downscaling over the land exceeded those over the ocean because of the underlying surface in regional model, which is different from the global model that produced the lateral boundary forcing (LBF).

Further, if we considered the added value only over the big lands (IC, Sumatra, Java, Borneo, and New Guinea, see Fig. 1 for definition) and neglected the small lands, the added values increased dramatically (Tab 3). In terms of the spatial correlation coefficient, the hindcast experiment showed added values over all the five big lands in MAM. In DJF, even though high spatial correlation coefficients were observed only over Sumatra, Java, and New Guinea, the averaged correlation

coefficients over the five big lands of the hindcast experiment were much higher than those in the EAR-40; this was not observed in the case of all the small islands in DJF. In both of JJA and SON, the averaged coefficient over the five big lands in the hindcast experiment was still higher than that in EAR-40.

Table 3 Spatial correlation coefficients (Rs) of seasonal precipitation of the ERA-40 and hindcast downscaling experiments relative to the observation in MAM, JJA, SON, and DJF, over IC, Sumatra, Java, Borneo, and New Guinea. The last column is the averaged Rs over the five regions.

Rs(GCM/RCM)	IC	Sumatra	Java	Borneo	New Guinea	average
MAM	0.34 \ 0.46	0.22 \ 0.46	-0.04 \ 0.58	0.01 \ 0.33	0.12 \ 0.27	0.13 \ 0.42
JJA	0.54 \ 0.37	0.40 \ 0.56	0.68 \ 0.66	0.22 \ 0.69	0.45 \ 0.56	0.46 \ 0.57
SON	0.69 \ 0.67	0.57 \ 0.59	0.21 \ 0.69	0.13 \ 0.61	0.45 \ 0.60	0.41 \ 0.63
DJF	0.85 \ 0.53	0.22 \ 0.64	0.23 \ 0.54	0.14 \ 0.02	-0.21 \ 0.25	0.25 \ 0.40

In terms of RMSE (Tab 4), except in JJA, SON, and DJF over IC and in MAM, JJA, and DJF over Borneo, the hindcast experiment showed added values in all the other cases. The experiment also showed added values when all the small islands were included, the WRF model showed high averaged RMSE values over the five big lands in all seasons.

Table 4 Spatial root mean square error (Es, in unit of mm d^{-1}) of seasonal precipitation of the ERA-40 and hindcast downscaling experiments relative to the observation in MAM, JJA, SON, and DJF, over IC, Sumatra, Java, Borneo, and New Guinea. The last column is the averaged Es over the five regions.

Es(GCM/RCM)	IC	Sumatra	Java	Borneo	New Guinea	average
MAM	2.39 \ 1.57	7.75 \ 2.36	2.29 \ 1.53	2.38 \ 2.56	11.72 \ 7.21	5.30 \ 3.04
JJA	3.43 \ 5.43	5.38 \ 1.57	1.13 \ 1.11	1.90 \ 2.33	9.67 \ 3.17	4.30 \ 2.72
SON	1.66 \ 2.40	6.57 \ 2.14	3.01 \ 1.23	2.72 \ 1.93	12.43 \ 6.40	5.28 \ 2.82
DJF	0.81 \ 1.19	6.23 \ 3.72	2.86 \ 2.03	2.56 \ 3.23	11.19 \ 9.32	4.73 \ 3.90

The added value increases when the small islands are neglected; this indicates that the worse performance of the WRF model over the small islands degraded its skill. This problem may be attributed to the relatively coarse model resolution in the primary stage of the CORDEX project. Thus, it is necessary to increase the resolution to improve the model performance.

The hindcast experiment also showed biases in low-level circulation fields; this was probably induced by the lack of air-sea interaction. Although the WRF model showed poor performance in simulating precipitation over the small islands, it does have reliable simulation skills over big lands owing to its better representation of the underlying surface when it was driven by the "perfect" lateral boundary forcing from the reanalysis dataset.

4.2 Historical experiment

1) Low-level circulation

Unlike to the ensemble mean of the three reanalysis datasets, the HadGEM2-AO produced a negative geopotential height bias at 850 mb pressure level over a large part of the domain with a westerly anomaly over the Indian Ocean in the Southern Hemisphere and an easterly anomaly over the equatorial Pacific in MAM (Fig. 3a). Another cyclonic anomaly was observed over the Indochina peninsula and the northern SCS. The historical downscaling experiment of the WRF model (control experiment) showed an enhanced negative geopotential height anomaly in the output of HadGEM2-AO over the western model domain concentrating over the southwestern conner in MAM. The easterly anomaly over the equatorial Pacific also intensified (Fig. 3b).

In JJA, the HadGEM2-AO produced a strong easterly anomaly accompanied by a negative geopotential height anomaly over the northern domain (Fig. 3c), which was enhanced in the control experiment where the area of height anomaly deeper than 20 m extended to the equator. Geopotential height anomalies deeper than 10 m were observed over most of the domain (Fig. 3d).

In SON, the HadGEM2-AO produced a positive geopotential height anomaly over the southwestern domain and a negative anomaly over the northeastern domain (Fig. 3e). In the control experiment, the negative anomaly in the HadGEM2-AO was shifted to the west and enhanced over the Indochina peninsula and the SCS. The positive anomaly in the HadGEM2-AO was reduced to a negative anomaly in the control experiment (Fig. 3f).

In DJF, the HadGEM2-AO produced a negative geopotential height anomaly around 110° E throughout the domain (Fig. 3g), which was enhanced in the control experiment and centered over the Indian Ocean around latitude 10° S. The easterly anomaly in the HadGEM2-AO over the equatorial Pacific shifted to the east in the control experiment (Fig. 3h).

Upon forcing by the output of HadGEM2-AO, which simulates surface temperature well (Baek et al 2013), the biases in low-level circulation in the control experiment were larger than the biases that originally existed in HadGEM2-AO. This is because the WRF model was unable to reduce the uncertainties in the LBF. Therefore, the biases in the control experiment were larger than those in the hindcast experiment forced by the reanalysis dataset. Under similar lower boundary forcing, the biases in the lateral boundary forcing (LBF) from the HadGEM2-AO was the main reason behind the deterioration in the performance of the WRF model in the control experiment.

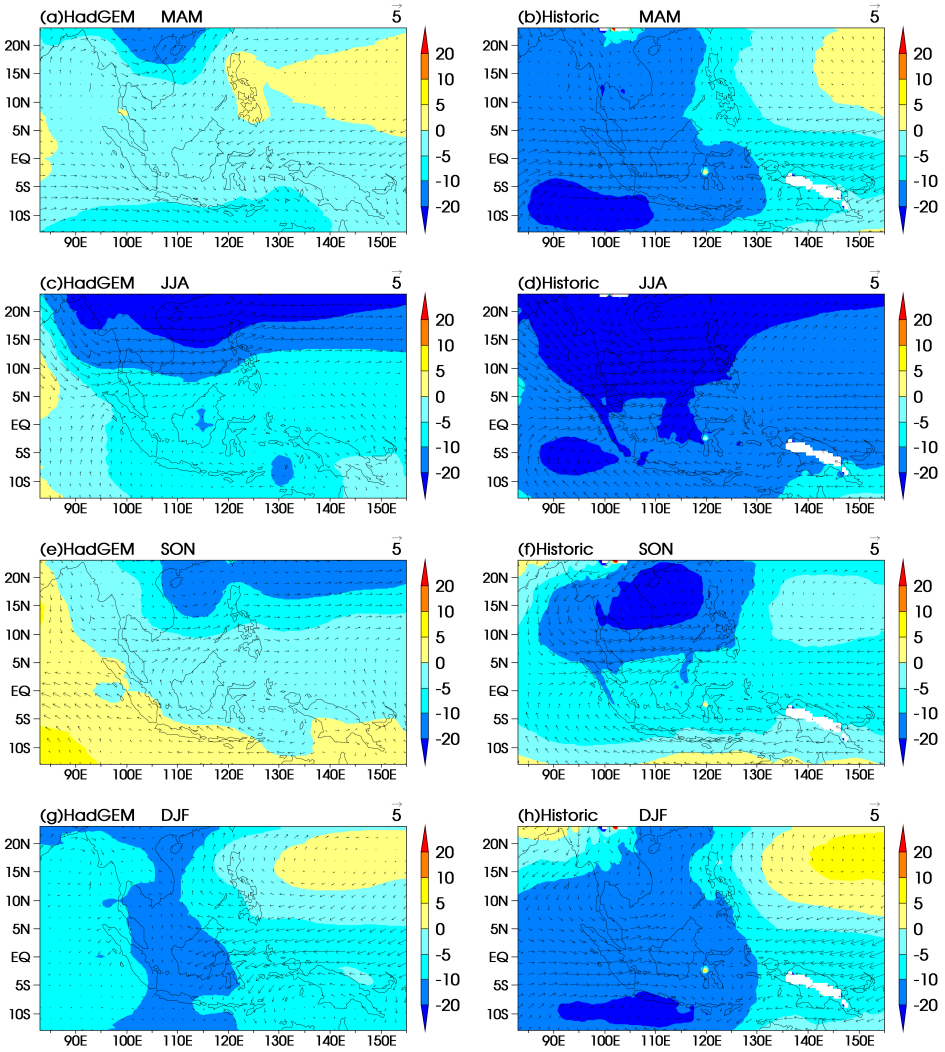

Figure 3 The model biases of geopotential height (shading in units of meter) and horizontal winds (vector in units of 5 m s^{-1}) at 850 hPa of the HadGEM2-AO and historical experiment in MAM mean (a, b), JJA mean (c, d), SON mean (e, f), and DJF mean (g, h). All the biases are defined by the departure of RCM simulations from the large-scale forcing of ensemble mean of the NCEP/DOE reanalysis 2 (NCEP-R2), ERA-40, and the Japanese 25-year reanalysis (JRA-25). White zones are the missing value masked by the topography.

2) Precipitation

The verification data of precipitation in the control experiment were the same as the verification data used in the hindcast experiment; the only difference between the two sets of data was that the period considered in the hindcast experiment was from 1971 to 2005.

To investigate the added value in the control experiment, we adopted four criteria calculated through the multi-year seasonal data from the output of the WRF model and its forcing, i.e., the HadGEM2-AO. For example, let r_{wrf} and r_{had} be the temporal correlation coefficients of the output of WRF and HadGEM2-AO relative to the verification precipitation. Let $r_t = r_{wrf} - r_{had}$; then, the positive value of r_t was the added value. Similarly, let e_{wrf} and e_{had} be the RMSE in the temporal dimension of the output from the WRF and HadGEM2-AO relative to the verification precipitation. Since $e_t = e_{had} - e_{wrf}$, the positive value of e_t represents the added value; this indicates that the WRF model had smaller RMSE than the RMSE of the HadGEM2-AO. Both r_t and e_t maps showed positive values indicating the added RMSE values. The other two criteria were calculated on the basis of the spatial dimensions of the seasonal data. Let r_{wrf}^{xy} and r_{had}^{xy} be the nine-point running correlation coefficients of one year's seasonal output of the WRF and HadGEM2-AO relative to the verification precipitation. Let $r_s = \overline{r_{wrf}^{xy}} - \overline{r_{had}^{xy}}$, where the bar represents the temporal average, then the positive value of r_s would be the added value. Let e_{wrf}^{xy} and e_{had}^{xy} be the absolute difference of one year seasonal output from the WRF and HadGEM2-AO relative to the verification precipitation, then $e_s = \overline{e_{had}^{xy}} - \overline{e_{wrf}^{xy}}$ would be positive if the WRF model reduced the absolute error of the HadGEM2-AO, where the bar represents the temporal average. The r_s and e_s maps showed positive values indicating the added values. In fact, e_t and e_s were interlinked, owing to which they were coherent.

The r_t shown in Fig. 4 indicates that the control experiment yielded added values over a large part of the Indochina peninsula and New Guinea, as well as over a

part of the Borneo Island in MAM. In JJA, the WRF model yielded added value of r_t over a part of the Indochina peninsula, Sumatra, Borneo, New Guinea, and entire Java. The amplitude of the added value in JJA was smaller than that in MAM. In SON, the added values were shown over northern part of the Indochina peninsula, large part of Borneo and Java. In DJF, added values are observed over southeastern part of the Indochina peninsula, large parts of Sumatra and Borneo, and the northern part of New Guinea.

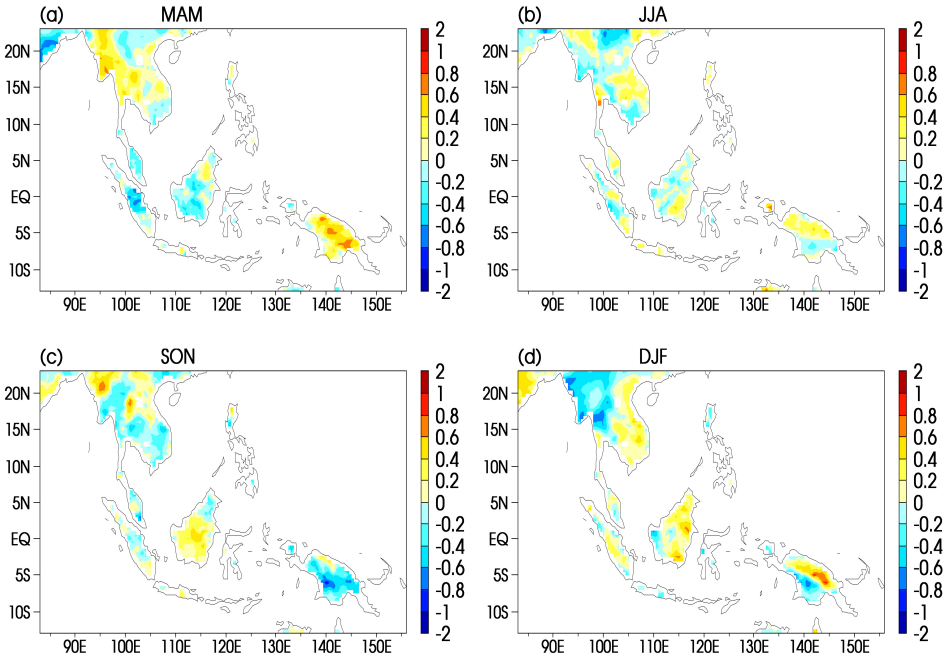

Figure 4 The difference between temporal correlation coefficients of the seasonal precipitation in historical experiment and HadGEM2-AO over land in MAM, JJA, SON, and DJF, relative to the verification precipitation. Positive value means the correlation coefficients of the historical experiment is larger than that of the HadGEM2-AO.

In terms of r_s (Fig. 5), the WRF model showed added values over the northern part and southwestern side of the Indochina peninsula, a part of Sumatra, Borneo, New Guinea, and most parts of Java in MAM. In JJA, the WRF model produced very high values over the central part of New Guinea and the northeastern part of the Indochina peninsula. Added values were also observed over parts of Sumatra and Java. In SON, added values were observed over most of the Indochina peninsula

and Sumatra. In New Guinea, added values were observed only over the central region with high topography. In DJF, added values were observed over a part of the Indochina peninsula, Java, Borneo, New Guinea, and most of Sumatra.

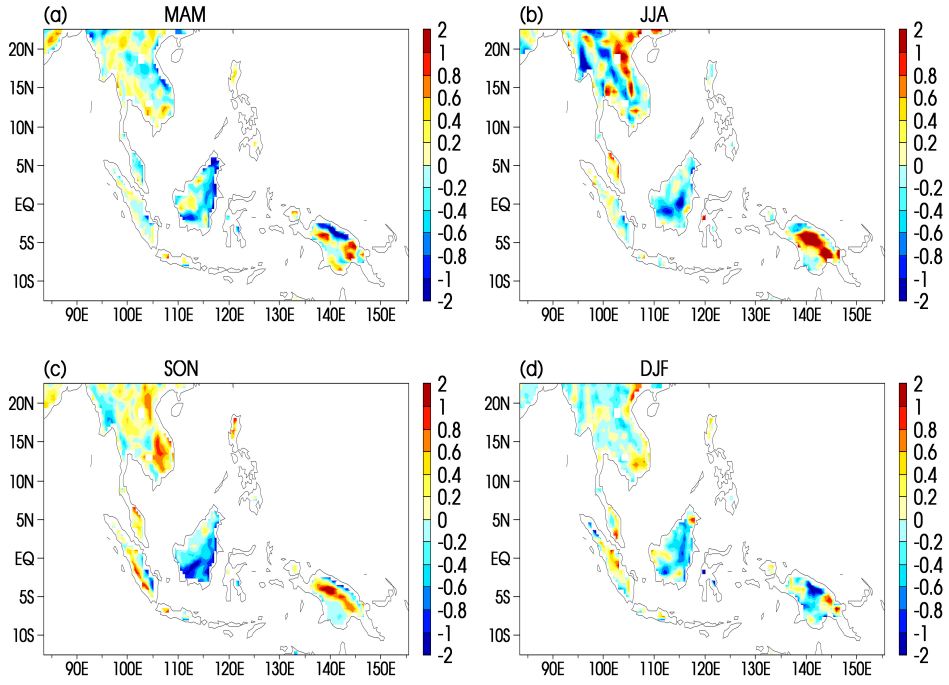

Figure 5 The difference between temporal averaged nine points spatial running correlation coefficients of the seasonal precipitation in historical experiment and HadGEM2-AO over land in MAM, JJA, SON, and DJF, relative to the verification precipitation. Positive value means the averaged correlation coefficients of the historical experiment is larger than that of the HadGEM2-AO.

In terms of e_t (Fig. 6), in MAM, the control experiment results showed added values over most parts of the Indochina peninsula, Sumatra, Borneo, and central southern part of New Guinea. In JJA, very high values were observed over the eastern Indochina peninsula and central New Guinea. Added values were also observed over parts of Sumatra and Borneo. In SON, the WRF model yielded added values over the southern Indochina peninsula, most parts of Borneo and Java, and parts of Sumatra and New Guinea. In DJF, the WRF model only produced added values over most of Java and parts of Sumatra, Borneo, and New Guinea. Over the Indochina peninsula, only a small region had added values of e_t.

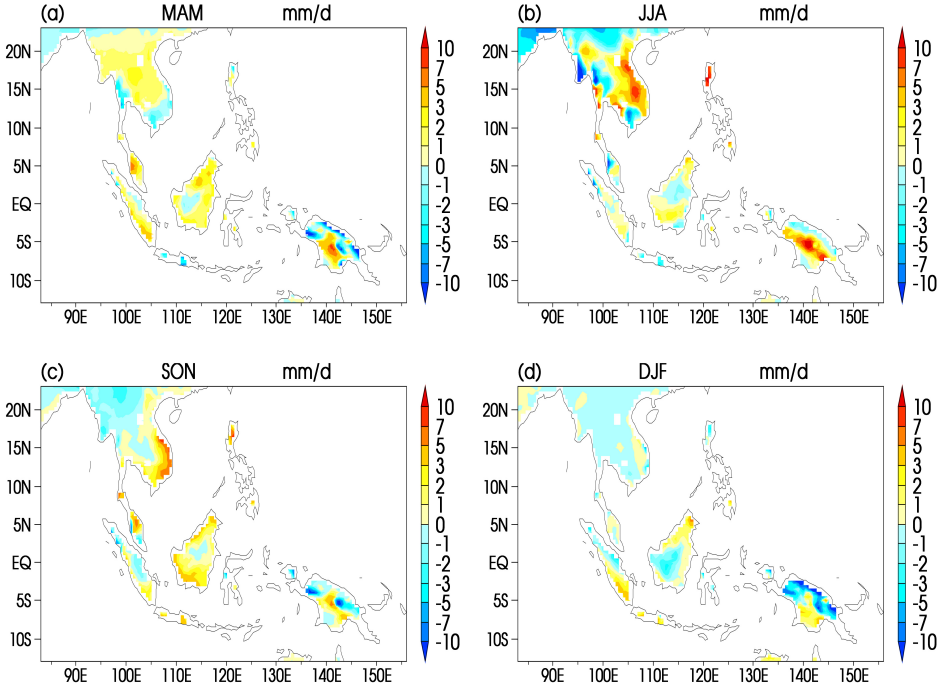

Figure 6 The difference between temporal root mean square errors of the seasonal precipitation in historical experiment and HadGEM2-AO over land in MAM, JJA, SON, and DJF, relative to the verification precipitation. Positive value means the root mean square errors of the historical experiment is less than that of the HadGEM2-AO.

Note that e_s and e_t have almost the same patterns and amplitudes.

The added value over the ocean was poor (figure not shown) owing to the biases in the LBF from the HadGEM2-AO and because of the lack of strong underlying forcing that may have been advantageous to the WRF model.

The low-level circulation bias from HadGEM2-AO was enhanced in the control experiment, while the precipitation bias in the former was reduced in the latter. The reduction was largely because of the strong forcing of the underlying surface; this forcing was better simulated in the control experiment than in the global HadGEM2-AO.

4.3 Future projection

1) Low-level circulation

We analyzed the low-level circulation changes in RCP4.5 and RCP8.5 projection for the periods 2021 to 2050 (near future) and 2071 to 2100 (far future) for the HadGEM2-AO and WRF simulations relative to their historical simulations.

In the near future of RCP4.5 projection in MAM (Fig. 7a), the change in geopotential height at the 850-hPa pressure level in the HadGEM2-AO was positive over the entire domain, with the largest change over the northern SCS and the northern Philippine Sea. The wind fields did not show any significant change. The downscaled result was consistent with HadGEM2-AO, with smaller increases in the geopotential height over the Philippine Sea (Fig. 7b). In the near future of RCP8.5 projection in MAM (Fig. 7c), HadGEM2-AO produced a larger increase in height than the increase produced in RCP4.5; the difference between the increases was especially noticeable over the ocean near the southern boundary. An easterly anomaly over the Indian Ocean was generated. The WRF model reproduced this change in the same way as in RCP4.5 (Fig. 7d).

In the far future of RCP4.5 projection in MAM (Fig. 7e), the geopotential height increased by more than 16 m over most part of domain with the largest increase at the northern boundary over the ocean and in the middle region of the southern boundary in the case of HadGEM2-AO. The WRF model produced a consistent change (Fig. 7f). The region with the maximum change near the southern boundary shifted to the west, and another region with positive changes was projected over the BOB and the Indochina peninsula in the WRF. The change in geopotential height was accompanied by an easterly anomaly over the Indian Ocean and southerly anomaly over the BOB in the WRF simulation. In the far future of RCP8.5 projection in MAM (Fig. 7g), HadGEM2-AO produced a positive change with a pattern similar to but larger in amplitude than in case of its near future projection. An easterly anomaly was generated over the Indian Ocean, a southerly anomaly over the BOB, and a westerly anomaly over the northern West Pacific. In the WRF model, the center of the region corresponding to the change near the southern boundary was shifted to the west,

and another region was generated over the BOB and the Indochina peninsula; this is similar to the modification made by the WRF model in case of RCP4.5 projection (Fig. 7h). The change in geopotential height was accompanied by the enhancement of an easterly anomaly over the Indian Ocean and a southerly anomaly over the BOB.

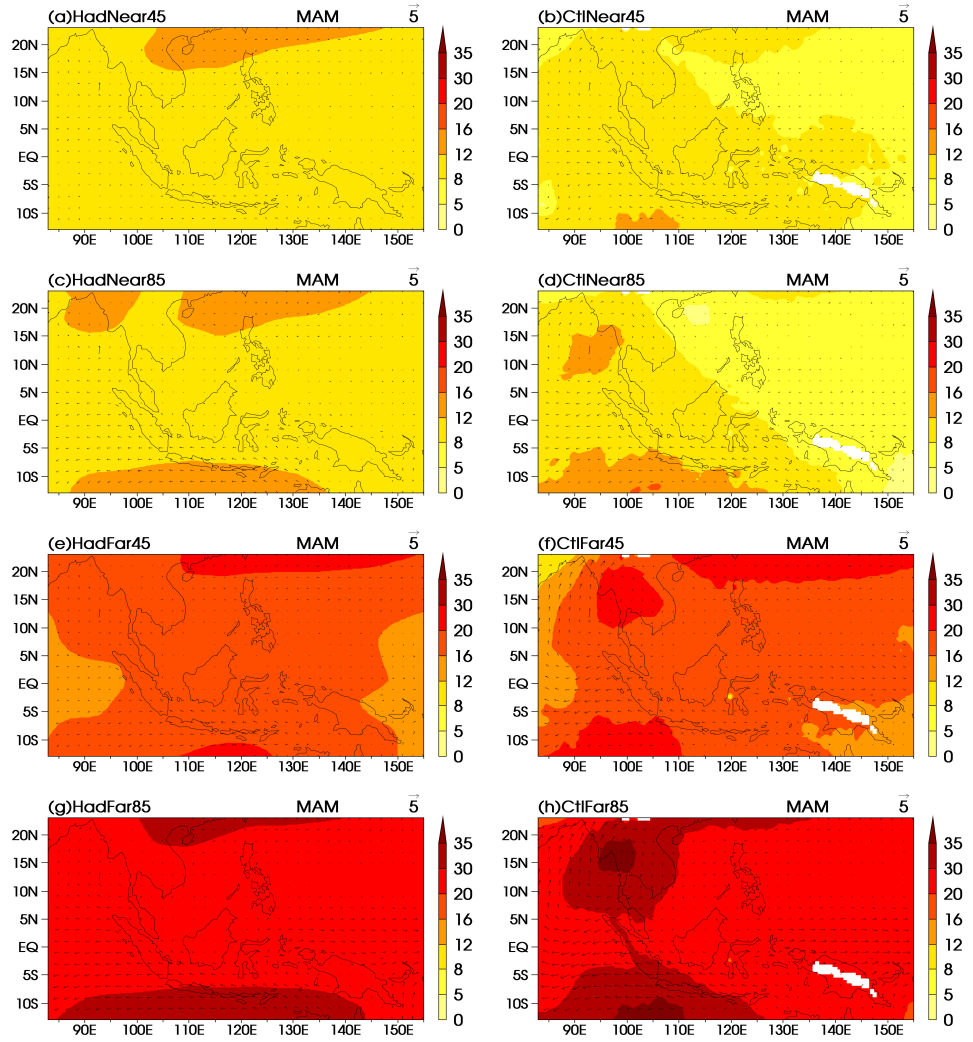

Figure 7 The near and far future changes of geopotential height (shading in units of meter) and horizontal winds (vector in units of 5 m s^{-1}) at 850 hPa of the HadGEM2-AO and WRF simulations in RCP4.5 and RCP8.5 in MAM. The changes are defined by the departure of each future simulation relative to its simulation of current climate. White zones are the missing value masked by the topography.

In the near future of RCP4.5 projection in JJA (Fig. 8a), HadGEM2-AO produced a positive change in the geopotential height at the 850-hPa pressure level over regions to the north of 10° N. The wind field did not show any significant change. The WRF model also reproduced this positive change in geopotential height over the entire domain. However, the change pattern was different. The WRF model produced the maximum change in the geopotential height over the BOB, a part of the Indian Ocean, and the North Pacific. A westerly anomaly was generated over the northern West Pacific (Fig. 8b). In the near future of RCP8.5 projection in JJA (Fig. 8c), HadGEM2-AO produced a positive change in geopotential height over the entire domain, with the largest change occurring over the BOB, the SCS, and the northern Philippine Sea. The positive change produced by the WRF model was different from that produced by HadGEM2-AO: the WRF model generated a large change over the entire Indian Ocean in the model domain. A westerly anomaly was also projected over the North Pacific by the WRF model (Fig. 8d).

In the far future of RCP4.5 projection in JJA (Fig. 8e), HadGEM2-AO produced a similar change as in the case of its near future projection, with the exception that the amplitude of the change was higher in the far future projection. The WRF model further enhanced this change and extended its range to most of the domain. An anticyclonic anomaly was also generated by the WRF model (Fig. 8f). In the far future of RCP8.5 projection in JJA (Fig. 8g), HadGEM2-AO produced a positive change in the geopotential height of > 30 m over most of the model domain with two high centers over the BOB and the SCS. An easterly anomaly was also shown to extend from the SCS to the northern Indian Ocean. The WRF model enhanced the easterly anomaly over the equatorial Indian Ocean by enhancing the anticyclone over the BOB and the Indochina peninsula; this increased the geopotential height by more than 35 m over a large area (Fig. 8h).

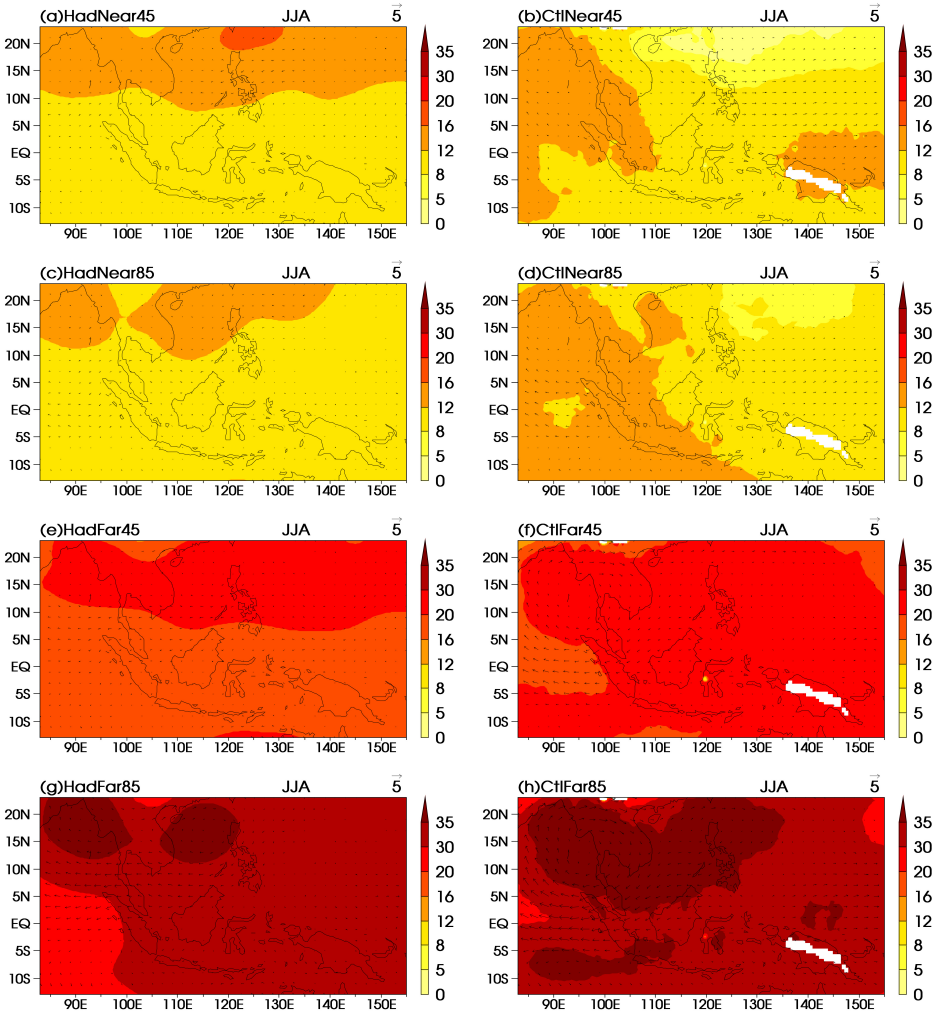

Figure 8 As in Fig. 7, but for JJA.

In the near future of RCP4.5 projection in SON (Fig. 9a), the HadGEM2-AO produced a uniform positive change in the geopotential height at the 850-hPa pressure level over the entire domain without any significant change in the wind field. The WRF model produced changes consistent with the HadGEM2-AO (Fig. 9b). In the near future of RCP8.5 projection in SON (Fig. 9c), the HadGEM2-AO produced a positive change in geopotential height over the entire domain with a high center over the Indochina peninsula and the SCS. The WRF model produced another high area corresponding

to a large change over the Indian Ocean in the southern hemisphere. The magnitude of change over the Indochina peninsula decreased, and an easterly anomaly was produced over the equatorial Indian Ocean (Fig. 9d).

In the far future of RCP4.5 projection in SON (Fig. 9e), HadGEM2-AO produced a positive change in the geopotential height over the entire domain with the change exceeding 16 m over most area and a northwesterly anomaly over the northern West Pacific. The WRF model shifted this pattern to the east and increased the height change over northern Philippines and the adjacent ocean (Fig. 9f). In the far future of RCP8.5 projection in SON (Fig. 9g), HadGEM2-AO produced a large positive change of more than 20 m in the geopotential height over most of the domain with a high center exceeding 30 m over the southern Indochina peninsula. A northwesterly anomaly occurred over the northern West Pacific. The produced pattern was slightly different in the case of the WRF model. A southwest northeast tilted area with a height change exceeding 30 m formed over the Indian Ocean, Sumatra, Borneo, the SCS, and Philippines. A strong anticyclonic anomaly was generated over the Indian Ocean at 10° N (Fig. 9h).

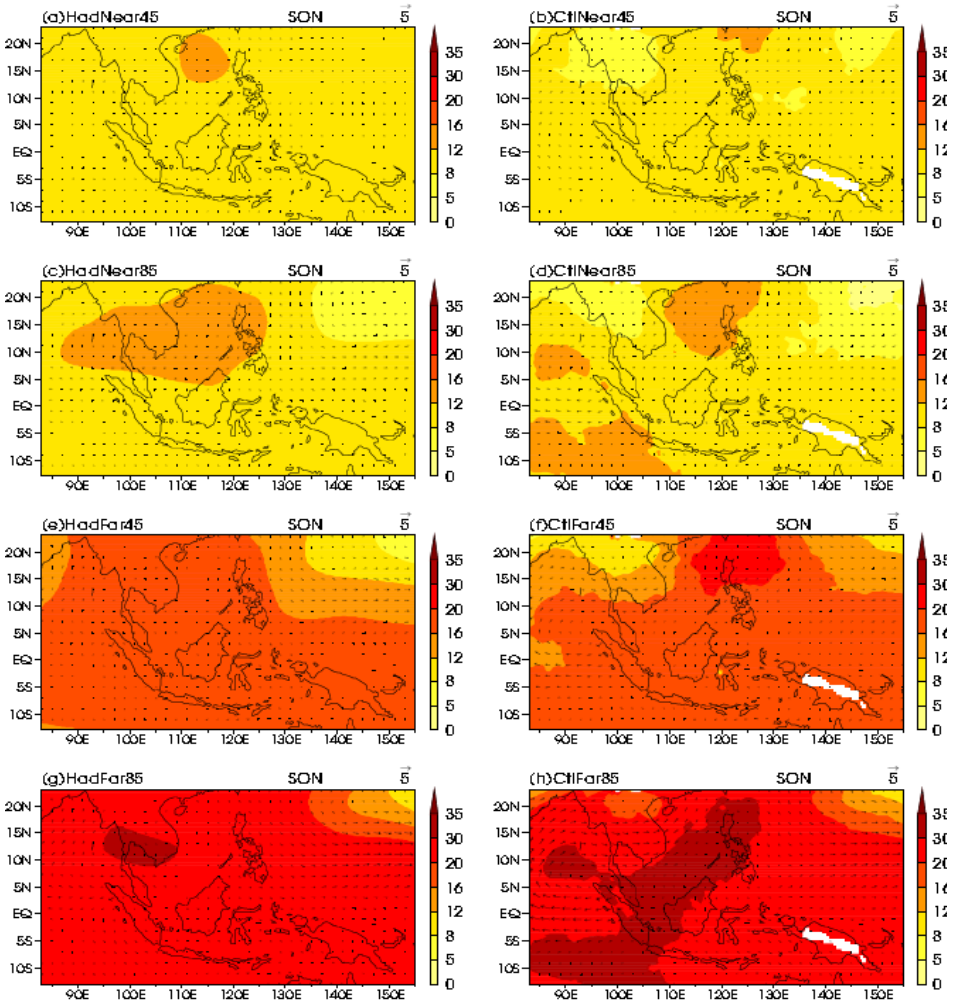

Figure 9 As same as Fig. 7, but for SON.

In the near future of RCP4.5 projection in DJF (Fig. 10a), HadGEM2-AO produced a uniform positive change in the geopotential height over entire domain. The pattern was almost the same in the case of the WRF model (Fig. 10b). In the near future of RCP8.5 projection in DJF (Fig. 10c), HadGEM2-AO produced a uniform positive change in geopotential height over the entire domain. The change in the geopotential height as produced by the WRF model was slightly higher over the Indian Ocean and lower over the West Pacific as compared to the corresponding changes in the case of HadGEM2-AO (Fig. 10d).

In the far future of RCP4.5 projection in DJF (Fig. 10e), the HadGEM2-AO produced a positive change of height over entire domain, with the largest value occurring near the northern boundary and smallest value over the Philippine Sea. The WRF model slightly modified this pattern by decreasing the change over the middle part of SEA (Fig. 10f). In the far future of RCP8.5 projection in DJF (Fig. 10g), HadGEM2-AO produced a uniform large positive change in height of more than 20 m over the entire domain. A northeasterly anomaly was generated over the ocean near the northern boundary and a southwesterly anomaly, over the equatorial Pacific. The WRF model reproduced the change pattern quite well and only enhanced the wind anomaly (Fig. 10h).

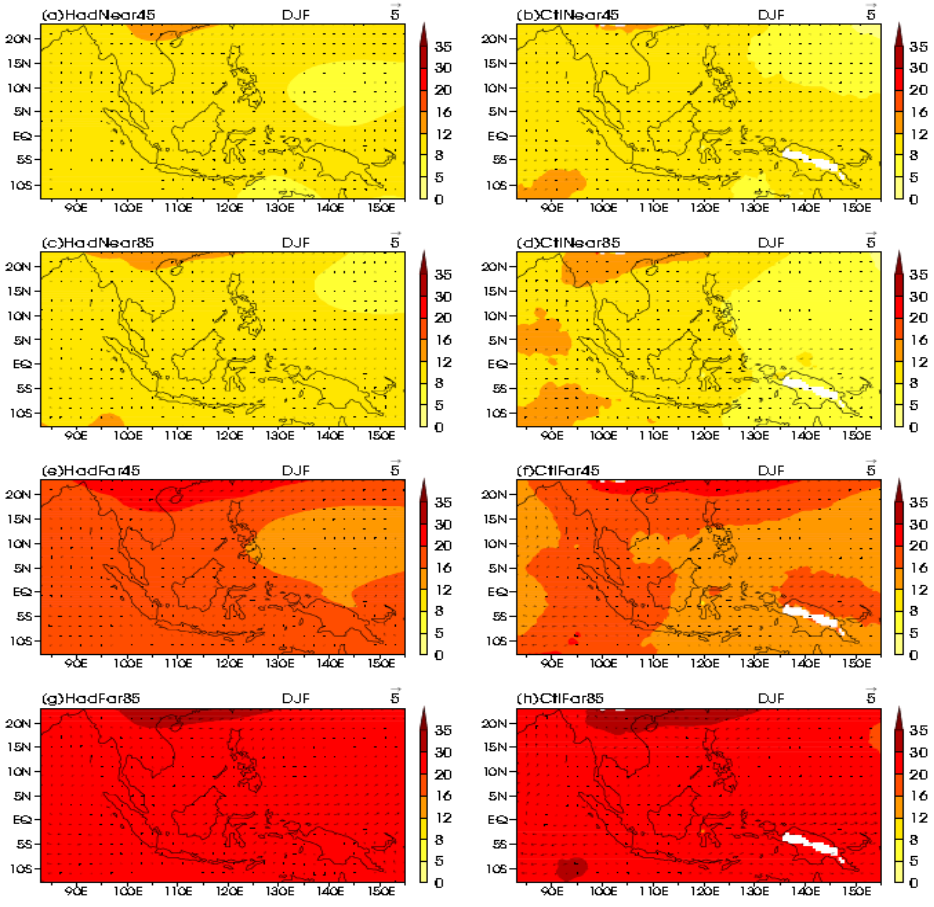

Figure 10 As same as Fig. 7, but for DJF.

2) Precipitation

We analyzed changes in precipitation in terms of the climatological seasonal mean and its spatial variability in RCP4.5 and RCP8.5 projection for 2021-2050 (near future) and 2071-2100 (far future) for both HadGEM2-AO and WRF simulations relative to their historical simulations.

The precipitation in the near future projection in RCP4.5 in MAM of both models was decreased over IC and increased over Borneo and New Guinea (Tab. 5). The change in the HadGEM2-AO simulation was enhanced over IC and weakened over Borneo and New Guinea by downscaling. The WRF model modified the sign of change in HadGEM2-AO simulation over Sumatra and Java. Except over Java, the changes of the precipitation variability in the HadGEM2-AO and WRF models were of the same sign—i.e., increasing over Borneo and New Guinea and decreasing over IC and Sumatra. In the far future of RCP4.5 projection in MAM (Tab. 5), HadGEM2-AO and WRF models produced similar precipitation changes over the five land regions, with the changes decreasing over IC and Java and increasing over Sumatra, Borneo, and New Guinea. The largest increase in precipitation occurred over New Guinea. In terms of spatial variability, the two models showed an increase in variability over Borneo and New Guinea, and a decrease in variability over IC and Sumatra. The WRF model enhanced the precipitation change over IC and New Guinea and weakened the precipitation change over Borneo, as evidenced by the changes in the mean and variability.

The precipitation in the near future projection in RCP8.5 in MAM of the both HadGEM2-AO and WRF models decreased over IC and Java and increased over New Guinea (Tab. 5). The change in the HadGEM2-AO simulation was enhanced over IC and weakened over New Guinea by downscaling. In the WRF model, the sign of change over Sumatra and Borneo was opposite to that in the case of the HadGEM2-AO simulation. The changes in the precipitation variability in the HadGEM2-AO and WRF models were of the same sign—i.e., increasing over IC and decreasing over New Guinea. The precipitation in the far future projection in RCP8.5 in MAM of the HadGEM2-AO model decreased over IC and Java and increased over Borneo (Tab. 5).

The changes over the above three land regions were enhanced by downscaling. In the WRF model, the sign of change over Sumatra and New Guinea was opposite to that in the case of the HadGEM2-AO simulation. Except over Java and New Guinea, the changes in the precipitation variability in the HadGEM2-AO and WRF models had the same sign-the changes increased over Borneo and decreased over IC and Sumatra.

Table 5 The near and far future changes of areal averaged climatological seasonal mean precipitation and its spatial variability (in units of mm d^{-1}) of the HadGEM2-AO and WRF simulations in RCP4.5 and RCP8.5 in MAM over IC, Sumatra, Java, Borneo, and New Guinea. The changes are defined by the departure of each future simulation relative to its simulation of current climate.

MAM RCP4.5 Near (HadGEM2_AO \ WRF)	IC	Sumatra	Java	Borneo	New Guinea
△Mean	-0.20 \ -0.31	-0.10 \ 0.25	0.01 \ -0.67	0.39 \ 0.18	0.92 \ 0.16
△Variance	-0.20 \ -2.43	-0.47 \ -0.59	0.15 \ -1.78	1.06 \ 1.19	2.81 \ 0.13

MAM RCP4.5 Far (HadGEM2_AO \ WRF)	IC	Sumatra	Java	Borneo	New Guinea
△Mean	-0.15 \ -0.30	0.65 \ 0.59	-0.44 \ -0.17	1.02 \ 0.53	1.58 \ 1.98
△Variance	-3.0e-03 \ -1.68	-0.03 \ -2.14	0.68 \ -0.36	1.84 \ 1.11	6.44 \ 20.15

MAM RCP8.5 Near (HadGEM2_AO \ WRF)	IC	Sumatra	Java	Borneo	New Guinea
△Mean	-0.33 \ -0.34	-0.37 \ 0.41	-1.44 \ -1.90	0.14 \ -0.02	0.75 \ 0.10
△Variance	-0.15 \ -1.70	-0.61 \ 0.74	0.31 \ -1.92	0.13 \ -0.23	8.19 \ 1.27

MAM RCP8.5 Far (HadGEM2_AO \ WRF)	IC	Sumatra	Java	Borneo	New Guinea
△Mean	-0.32 \ -0.91	-0.70 \ 0.56	-1.68 \ -2.64	0.11 \ 0.42	1.28 \ -0.18
△Variance	-0.31 \ -4.24	-0.25 \ -4.69	0.69 \ -3.77	0.10 \ 0.78	17.16 \ -2.79

In the case of near future projection in RCP4.5 in JJA (Tab. 6), the sign of the change produced by the WRF model was opposite to that in the case of the HadGEM2-AO simulation over all five land regions. However, the changes in the

precipitation variability in the HadGEM2-AO and WRF models had the same sign—they increased over Java and decreased over Sumatra.

The precipitation in the far future projection in RCP4.5 in JJA of HadGEM2-AO and WRF models decreased over Java and increased over IC (Tab. 6). The change in the HadGEM2-AO simulation was enhanced over both the abovementioned regions by downscaling. For the other three regions, the WRF model and HadGEM2-AO simulations yielded changes that differed in sign. The changes in the precipitation variability in the HadGEM2-AO and WRF models were of the same sign—increasing over IC and New Guinea. The precipitation in the near future projection in RCP8.5 in JJA of HadGEM2-AO and WRF models increased over IC and decreased over Sumatra, Java, Borneo, and New Guinea (Tab. 6). The change in the HadGEM2-AO simulation was weakened over Sumatra and enhanced over IC, Java, Borneo, and New Guinea by downscaling. The changes in the precipitation variability in the HadGEM2-AO and WRF models were of the same sign—that is, increasing over IC and decreasing over Java.

The precipitation in the far future projection in RCP8.5 in JJA of HadGEM2-AO and WRF models decreased over Sumatra, Java, Borneo, and New Guinea (Tab. 6). The change in the HadGEM2-AO simulation over these four lands was enhanced by downscaling. The WRF model modified the sign of change in the HadGEM2-AO simulation over IC. The changes in the precipitation variability in the HadGEM2-AO and WRF models were of the same sign—i.e., increasing over IC and decreasing over Java.

Table 6 As same as Table 5, but for JJA.

JJA RCP4.5 Near (HadGEM2_AO \ WRF)	IC	Sumatra	Java	Borneo	New Guinea
△Mean	-0.18 \ 0.37	0.03 \ -0.40	-0.12 \ 1.60	0.52 \ -0.80	0.49 \ -0.64
△Variance	-1.58 \ 4.15	-3.4e-03 \ -2.89	0.14 \ 1.22	0.23 \ -3.27	3.62 \ -6.78

JJA RCP4.5 Far (HadGEM2_AO \ WRF)	IC	Sumatra	Java	Borneo	New Guinea
△Mean	0.07 \ 0.48	0.19 \ -0.11	-0.52 \ -0.95	0.85 \ -0.41	0.40 \ -0.60
△Variance	1.86 \ 12.90	0.72 \ -6.93	0.06 \ -1.51	0.89 \ -2.68	4.69 \ 1.05

JJA RCP8.5 Near (HadGEM2_AO \ WRF)	IC	Sumatra	Java	Borneo	New Guinea
△Mean	0.04 \ 0.06	-0.44 \ -0.22	-0.81 \ -0.83	-0.19 \ -0.65	-0.05 \ -1.59
△Variance	0.61 \ 5.11	0.57 \ -3.74	-0.17 \ -0.73	0.65 \ -3.52	1.62 \ -12.92

JJA RCP8.5 Far (HadGEM2_AO \ WRF)	IC	Sumatra	Java	Borneo	New Guinea
△Mean	-0.42 \ 0.27	-0.76 \ -1.00	-1.12 \ -3.34	-0.08 \ -0.96	-0.18 \ -1.14
△Variance	5.29 \ 8.46	1.24 \ -12.52	-0.33 \ -2.38	1.91 \ -3.23	2.42 \ -9.07

The precipitation in the near future projection in RCP4.5 in SON of HadGEM2-AO and WRF models decreased over Sumatra and Java and increased over IC and New Guinea (Tab. 7). The change in the HadGEM2-AO simulation was enhanced over IC and Java and weakened over Sumatra and New Guinea by downscaling. The WRF model modified the sign of change in HadGEM2-AO simulation over Borneo. Except over Sumatra and Borneo, the changes in the precipitation variability in the HadGEM2-AO and WRF models were of the same sign—i.e., decreasing over Java and increasing over IC and New Guinea. The precipitation in the far future projection in RCP4.5 in SON of HadGEM2-AO and WRF models decreased over Sumatra and Java and increased over IC, Borneo, and New Guinea (Tab. 7). The change in the HadGEM2-AO simulation was enhanced over all the five regions by downscaling. Except over Sumatra, the changes in the precipitation variability in the HadGEM2-AO and WRF models were of the same sign—i.e., they decreased over Java and increased over IC, Borneo, and New Guinea.

The precipitation in the near future projection in RCP8.5 in SON of HadGEM2-AO and WRF models increased over IC and decreased over Sumatra and Borneo (Tab. 7). The change in the HadGEM2-AO simulation was weakened over Borneo and enhanced over IC and Sumatra by downscaling. The WRF model modified the sign of change in the HadGEM2-AO simulation over Java and New Guinea. The changes in the precipitation variability in the HadGEM2-AO and WRF models were of the same sign-that is, decreasing only over Borneo. The precipitation in the far future projection in RCP8.5 in SON in HadGEM2-AO and WRF models increased over IC and decreased over Sumatra, Java, and Borneo (Tab. 7). The change in the HadGEM2-AO simulation was enhanced over IC and Sumatra and weakened over Java and Borneo by downscaling. The WRF model modified the sign of change in HadGEM2-AO simulation over New Guinea. Except over IC and Sumatra, the changes in the precipitation variability in the HadGEM2-AO and WRF models were of the same sign, i.e., decreasing over Java and increasing over Borneo and New Guinea.

Table 7 As same as Table 5, but for SON.

SON RCP4.5 Near (HadGEM2_AO \ WRF)	IC	Sumatra	Java	Borneo	New Guinea
△Mean	0.38 \ 1.09	-0.63 \ -0.26	-0.06 \ -0.17	-0.26 \ 0.11	0.64 \ 0.26
△Variance	0.43 \ 9.64	-2.20 \ 5.90	-0.07 \ -0.10	-0.68 \ 1.38	4.42 \ 3.75

SON RCP4.5 Far (HadGEM2_AO \ WRF)	IC	Sumatra	Java	Borneo	New Guinea
△Mean	0.51 \ 1.93	-0.39 \ -0.99	-0.17 \ -0.21	3.2e-03 \ 0.42	0.49 \ 0.66
△Variance	0.13 \ 10.98	3.18 \ -6.11	-0.04 \ -0.13	0.55 \ 4.52	2.70 \ 7.69

SON RCP8.5 Near (HadGEM2_AO \ WRF)	IC	Sumatra	Java	Borneo	New Guinea
△Mean	0.15 \ 1.26	-0.98 \ -1.95	-0.38 \ 0.32	-0.61 \ -0.21	-0.31 \ 0.04
△Variance	-0.38 \ 6.15	1.19 \ -19.98	-0.12 \ 0.01	-1.01 \ -0.14	1.26 \ -4.00

SON RCP8.5 Far (HadGEM2_AO \ WRF)	IC	Sumatra	Java	Borneo	New Guinea
△Mean	0.73 \ 2.75	-2.08 \ -3.54	-0.58 \ -0.53	-1.10 \ -0.71	-0.19 \ 1.25
△Variance	-0.03 \ 12.07	1.22 \ -20.59	-0.18 \ -0.74	0.12 \ 1.43	2.00 \ 2.10

The precipitation in the near future projection in RCP4.5 in DJF of HadGEM2-AO and WRF models decreased over Java and Borneo (Tab. 8). The change in the HadGEM2-AO simulation was enhanced over Java and weakened over Borneo by downscaling. The WRF model modified the sign of change in HadGEM2-AO simulation over IC, Sumatra, and New Guinea. Except over Borneo and New Guinea, the changes in the precipitation variability in the HadGEM2-AO and WRF models were of the same sign, i.e., decreasing over Java and increasing over IC and Sumatra. The precipitation in the far future projection in RCP4.5 in DJF of HadGEM2-AO and WRF models decreased over Java and increased over IC and Borneo (Tab. 8). The change in the HadGEM2-AO simulation was weakened over Borneo and enhanced over IC and Java by downscaling. The WRF model modified the sign of change in HadGEM2-AO simulation over Sumatra and New Guinea. Except IC, where the precipitation variability increased in both models, the models projected variabilities of opposite signs over the other four big land regions.

The precipitation in the near future projection in RCP8.5 in DJF of HadGEM2-AO and WRF models increased over IC and decreased over Sumatra, Java, and New Guinea (Tab. 8). The change in the HadGEM2-AO simulation was weakened over Sumatra and enhanced over IC, Java, and New Guinea by downscaling. The WRF model modified the sign of change in HadGEM2-AO simulation over Borneo. Except Sumatra, where the precipitation variability decreased for both the models, the models projected variability changes of opposite signs over the other four big land regions. The precipitation in the far future projection in RCP8.5 in DJF of the both HadGEM2-AO and WRF models increased over IC and decreased over Sumatra, Java, Borneo, and New Guinea (Tab. 8). The change in the HadGEM2-AO simulation was weakened over Sumatra and enhanced over IC, Java, Borneo, and New Guinea by downscaling. Except Sumatra, where both models projected a decrease in precipitation variability, the models projected changes of opposite signs in variability over the other four big land regions.

Table 8 As same as Table 5, but for DJF.

DJF RCP4.5 Near (HadGEM2_AO \ WRF)	IC	Sumatra	Java	Borneo	New Guinea
△Mean	-0.04 \ 0.10	-1.8e-04 \ 0.11	-0.15 \ -2.66	-0.09 \ -0.02	0.37 \ -1.70
△Variance	0.02 \ 0.85	0.14 \ 3.41	-0.20 \ -0.48	-0.68 \ 2.55	0.83 \ -21.95

DJF RCP4.5 Far (HadGEM2_AO \ WRF)	IC	Sumatra	Java	Borneo	New Guinea
△Mean	0.12 \ 0.27	0.73 \ -2.9e-03	-0.26 \ -2.50	0.71 \ 0.27	0.34 \ -0.61
△Variance	0.24 \ 1.27	-0.03 \ 0.56	-0.05 \ 4.97	-1.68 \ 3.98	2.45 \ -19.46

DJF RCP8.5 Near (HadGEM2_AO \ WRF)	IC	Sumatra	Java	Borneo	New Guinea
△Mean	0.02 \ 0.25	-0.94 \ -0.68	-1.17 \ -2.63	-0.28 \ 0.01	-0.21 \ -0.94
△Variance	-0.40 \ 1.38	-0.22 \ -3.36	0.04 \ -1.62	-3.12 \ 2.81	4.87 \ -21.56

DJF RCP8.5 Far (HadGEM2_AO \ WRF)	IC	Sumatra	Java	Borneo	New Guinea
△Mean	0.19 \ 0.54	-0.77 \ -0.77	-1.43 \ -2.39	-6.4e-04 \ -0.07	-0.32 \ -1.68
△Variance	-0.39 \ 2.98	-0.44 \ -2.04	-0.21 \ 0.06	-3.91 \ 4.29	6.09 \ -29.51

Over all, the largest discrepancy between the HadGEM2-AO and WRF models in terms of sign of mean precipitation change occurred in JJA in RCP4.5; in other words, the uncertainty in RCP4.5 projection for JJA was the largest among all the cases. The mean precipitation change in the HadGEM2-AO model was more likely enhanced by the WRF model in the far future than in the near future. The projected precipitation variability of the two models differed more frequently than did their projected mean precipitation; this suggests that the uncertainty in the projection of precipitation variability was larger than that in the projection of mean precipitation.

5. CONCLUSION

In order to study the impact of climate change on hydrological and agricultural sectors over the Maritime Continent, four regional climate dynamic downscaling experiments have been carried out with the WRF model. The hindcast and historical downscaling experiments for current climate have been forced by reanalysis data and global model output, respectively. Two climate change downscaling experiments have been driven by the global model projections. This study provides the preliminary results and an insight into the dynamic downscaling approach for policy planning, agricultural productivity management, and management of the water resources.

The added values of dynamic downscaling over the land exceeds that over the ocean because an underlying surface is considered in the regional model, unlike the global model that produces the LBF.

The added value further increased when small islands are neglected, indicating that the poor performance of the WRF model over the small islands degrades its skill. The relatively coarse model resolution in the primary strategy of the CORDEX project is responsible for this deficiency. Thus, it is necessary to increase the resolution to improve the model performance.

Even though the hindcast experiment has biases in low-level circulation fields and shows poor performance in simulating the precipitation over the small islands, the WRF model does have sufficient skill in simulating the conditions for the big land regions owing to its better representation of the underlying surface when it is driven by the “perfect” lateral boundary forcing from the reanalysis dataset.

When forced by the output of HadGEM2-AO, the biases in low-level circulation in the control experiment were larger than the originally existed biases in the HadGEM2-AO because the WRF model did not reduce the uncertainties in the LBF. Therefore, the biases in the control experiment were larger than those in the hindcast experiment forced by the reanalysis dataset. Under the same model configuration, the biases in the LBF from the HadGEM2-AO were the main reason for the worsening of the performance of the WRF model in the control experiment.

The added value over the ocean is poor (figure not shown) owing to the biases in the LBF from the HadGEM2-AO as well as the lack of strong underlying forcing.

The low-level circulation bias from the HadGEM2-AO is enlarged in the control experiment, whereas the precipitation bias in the former is reduced in the latter. The reducing is largely attributed to the strong forcing from the underlying surface that is better simulated in the control experiment than in the global HadGEM2-AO.

Over all, the largest discrepancy between the HadGEM2-AO and WRF models in terms of the sign of mean precipitation change occurred in JJA in the RCP4.5 projection. That is, the uncertainty in the RCP4.5 projection for JJA was the highest. The mean precipitation change in HadGEM2-AO model was more likely enhanced by the WRF model in the far future than in the near future. The projected precipitation variability of the two models differed more frequently than did their projected mean precipitation values. This suggests that the uncertainty in the projection of precipitation variability is larger than that in the projection of mean precipitation.

Owing to the limitation of the available computational resources, our experiments use relatively coarse resolution data, and this degraded the model performance over the small islands. A 25 km experiments are under planning. The bias in the prescribed SST from the large-scale model persists throughout the entire period of our downscaling experiments and influences the thermodynamic balance of the circulation since air-sea interaction has not been considered. A coupled regional climate model help solve this problem. The bias originating from LBF also need be reduced in the next work; this can be done by using quintile mapping or the Bayesian Model Averaging methods.

REFERENCES

Adler R. F., G. J. Huffman, D. T. Bolvin et al., 2000: Tropical rainfall distributions determined using TRMM combined with other satellite and rain gauge information. *J. Appl. Meteorol.,* **39**, 2007-2023.

Adler R. F., G. J. Huffman, A. Chang, et al., 2003: The version-2 global precipitation climatology project (GPCP) monthly precipitation analysis (1979-present). *J. Hydrometeorol.,* **4**, 1147-1167.

Baek, H. J. and coauthors, 2013: Climate change in the 21st century simulated by HadGEM2-AO under representative concentration pathways. Asia-Pacific Journal of Atmospheric Sciences, 1-16.

Beljaars, A.C.M., 1994: The parameterization of surface fluxes in large-scale models under free convection. *Quart. J. Roy. Meteor. Soc.,* **121**, 255-270.

Boyle, J., and S. A. Klein, 2010: Impact of horizontal resolution on climate model forecasts of tropical precipitation and diabatic heating for the TWP-ICE period. *Journal of Geophysical Research: Atmospheres* (1984-2012), 115(D23).

Chang, C. P., P. A. Harr, AND H. J. Chen, 2005: Synoptic disturbances over the equatorial South China Sea and western Maritime Continent during boreal winter. *Monthly Weather Review*, **133**(3), 489-503.

Collins, William D., et al., 2004: Description of the NCAR Community Atmosphere Model (CAM 3.0). NCAR Tech. Note NCAR/TN-464+STR. 214 pp.

Dirmeyer, P. A., B. A. Cash, J. L. Kinter III, T. Jung, L. Marx, L., M. Satoh, ... and J. Manganello, 2012: Simulating the diurnal cycle of rainfall in global climate models: resolution versus parameterization. *Climate Dynamics*, **39**(1-2), 399-418.

Dyer, A. J., and B. B. Hicks, 1970: Flux-gradient relationships in the constant flux layer. *Quart. J. Roy. Meteor. Soc.*, **96**, 715-721.

Fu, X., B. Wang, and T. Li, 2002: Impacts of Air-Sea Coupling on the Simulation of Mean Asian Summer Monsoon in the ECHAM4 Model*. *Monthly Weather Review*, **130**(12), 2889-2904.

Fu, X., and B. Wang, 2004: Differences of Boreal Summer Intraseasonal Oscillations Simulated in an Atmosphere-Ocean Coupled Model and an Atmosphere-Only Model. *J. of Climate*, **17**, 1263-1271

Hong, S.-Y., J. Dudhia, and S.-H. Chen, 2004: A Revised Approach to Ice Microphysical Processes for the Bulk Parameterization of Clouds and Precipitation. *Mon. Wea. Rev.,* **132**, 103-120.

Hong, Song-You, Yign Noh, Jimy Dudhia, 2006: A new vertical diffusion package with an explicit treatment of entrainment processes. *Mon. Wea. Rev.,* **134**, 2318-2341.

Huffman, G. J., and Coauthors, 2007: The TRMM Multisatellite Precipitation Analysis (TMPA): Quasi-global, multiyear, combined-sensor precipitation estimates at fine scales. *J. Hydrometeor.,* **8**, 38-55.

Ichikawa, Hiroki, Tetsuzo Yasunari, 2008: Intraseasonal Variability in Diurnal Rainfall over New Guinea and the Surrounding Oceans during Austral Summer. *J. Climate*, **21**, 2852-2868.

Kikuchi, K., and B. Wang, 2008: Diurnal precipitation regimes in the global tropics*. *Journal of Climate*, **21**(11), 2680-2696.

Love, B. S., A. J. Matthews, and G. Lister, 2011: The diurnal cycle of precipitation over the Maritime Continent in a high-resolution atmospheric model. *Quarterly Journal of the Royal Meteorological Society*, **137**(657), 934-947.

New, M., D. Lister, M. Hulme, and I. Makin, 2002: A high-resolution data set of surface climate over global land areas. *Clim. Res.,* **21**(1), 1-25.

Neale, R., and J. Slingo, 2003: The maritime continent and its role in the global climate: A GCM study. *Journal of Climate,* **16**(5), 834-848.

Mori, S., H. Jun-Ichi, Y. I. Tauhid, M. D. Yamanaka, N. Okamoto, F. Murata, ... and T. Sribimawati, 2004: Diurnal land-sea rainfall peak migration over Sumatera Island, Indonesian maritime continent, observed by TRMM satellite and intensive rawinsonde soundings. *Monthly Weather Review,* **132**(8), 2021-2039.

Paulson, C. A., 1970: The mathematical representation of wind speed and temperature profiles in the unstable atmospheric surface layer. *J. Appl. Meteor.,* **9**, 857-861.

Peatman, S. C., A. J. Matthews, and D. P. Stevens, 2013: Propagation of the Madden-Julian Oscillation through the Maritime Continent and scale interaction with the diurnal cycle of precipitation. *Quarterly Journal of the Royal Meteorological Society.*

Qian, J. H., 2008: Why precipitation is mostly concentrated over islands in the Maritime Continent. *Journal of the Atmospheric Sciences,* **65**(4), 1428-1441.

Qian, J. H., and L. Zubair, 2010. The effect of grid spacing and domain size on the quality of ensemble regional climate downscaling over South Asia during the northeasterly monsoon. *Monthly Weather Review,* **138**(7), 2780-2802.

Qian, J. H., A. W. Robertson, and V. Moron, 2010: Interactions among ENSO, the monsoon, and diurnal cycle in rainfall variability over Java, Indonesia. *Journal of the Atmospheric Sciences,* **67**(11), 3509-3524.

Sato, T., H. Miura, M. Satoh, Y. N. Takayabu, and Y. Wang, 2009: Diurnal cycle of precipitation in the tropics simulated in a global cloud-resolving model. *Journal of Climate,* **22**(18), 4809-4826.

Smith, I., A. Moise, J. Katzfey, K. Nguyen, and R. Colman, 2013: Regional-scale rainfall projections: Simulations for the New Guinea region using the CCAM model. *Journal of Geophysical Research: Atmospheres*.

Susan, S. (Ed.). (2007). Climate change 2007-the physical science basis: Working group I contribution to the fourth assessment report of the IPCC (Vol. 4). Cambridge University Press.

Tewari, M., F. Chen, W. Wang, J. Dudhia, M. A. LeMone, K. Mitchell, M. Ek, G. Gayno, J. Wegiel, and R. H. Cuenca, 2004: Implementation and verification of the unified NOAH land surface model in the WRF model. 20th Conference on Weather Analysis and Forecasting/16th Conference on Numerical Weather Prediction, pp. 11-15.

Tiedtke, M., 1989: A comprehensive mass flux scheme for cumulus parameterization in large-scale models. *Mon. Wea. Rev.,* **117**, 1779-1800.

Uppala, S. M. and coauthors, 2005: The ERA-40 re-analysis. *Quarterly Journal of the Royal Meteorological Society,* **131**(612), 2961-3012.

Webb, E. K., 1970: Profile relationships: The log-linear range, and extension to strong stability. Quart.

J. Roy. Meteor. Soc., 96, 67-90.

Wu, C. H., and H. H. Hsu, 2009: Topographic influence on the MJO in the Maritime Continent. *Journal of Climate,* **22**(20), 5433-5448.

Xie P., and P. A. Arkin, 1996: Global precipitation: A 17-year monthly analysis based on gauge observations, satellite estimates, and numerical model outputs. *Bull. Am. Meteor. Soc.,* **78**:2539-2558

Yatagai, A., O. Arakawa, K. Kamiguchi, H. Kawamoto, M. I. Nodzu, and A. Hamada, 2009: A 44-year daily gridded precipitation dataset for Asia based on a dense network of rain gauges. *Sola*, **5**(0), 137-140.

Zhang, Chunxi, Yuqing Wang, and Kevin Hamilton, 2011: Improved representation of boundary layer clouds over the southeast pacific in ARW-WRF using a modified Tiedtke cumulus parameterization scheme. *Mon. Wea. Rev.,* **139**, 3489-3513.

Zhang, D.-L., and R.A. Anthes, 1982: A high-resolution model of the planetary boundary layer- sensitivity tests and comparisons with SESAME-79 data. *J. Appl. Meteor.,* **21**, 1594-1609.

Zhou, L., and Y. Wang, 2006: Tropical Rainfall Measuring Mission observation and regional model study of precipitation diurnal cycle in the New Guinean region. *Journal of Geophysical Research: Atmospheres* (1984-2012), 111(D17).

APCC RESEARCH REPORT 2013-02

- Construction of BSISO Forecast System and Application to Summer Monsoon Prediction
- Revision of Climate Change by Dynamic Downscaling over the Maritime Continents
- Long-Lead Station-Scaled Prediction of a Hydrological Drought in South Korea Based on Bivariate Downscaling
- Development of Scaled SVD Analysis and Related Methods with Focus on Application to Tropical-Extratropical Teleconnections

APEC Climate Center

12, Centum 7-ro, Haeundae-gu, Busan 612-020,
Republic of Korea
Tel: +82-51-745-3900 Fax: +82-51-745-3949
www.apcc21.org

비매품
94550
9 788997 333943
ISBN 978-89-97333-94-3
ISBN 978-89-97333-92-9 (세트)